Enclosure and Conductive Effects on Thermal Performance of Liquid Droplet Radiators

Yildiz Bayazitoglu* and Peter D. Jones†
Rice University, Houston, Texas 77004

Heat rejection from rectangular-type liquid droplet radiators, bounded by enclosures and including a conductive gas among the droplets, is studied. A numerical solution based on the P_1 approximation is used. An analytical solution based on fully developed temperature profiles compares well with the numerical simulation. It is found that enclosures of transmissive/emissive materials reduce the heat-rejection capability of a liquid droplet radiator as a function of a single parameter of the enclosure radiative properties. Cases with gas conduction show a general flattening of the temperature profile across the layer. The effect of conduction on the overall heat rejection of the layer depends on the enclosure materials. For fully transmissive enclosures there is negligible overall effect. For emissive (black) enclosures, there is a strong effect for higher conduction-to-radiation ratios.

Nomenclature

c_p = specific heat of gas-liquid mixture, J/kgK
C = enclosure parameter, $=\rho_w + \epsilon_w/2$
D = droplet diameter, m
G = incident radiation, w/m^2
I = radiation intensity, w/m^2
k = thermal conductivity of gas, w/mK
M = separation constant, w/m^2
m = nonconducting profile constant
N = conduction-to-radiation ratio, $=\beta k/\sigma T_i^3$
n = droplet number density, m^{-3}
Q_a = absorption efficiency
Q_s = scattering efficiency
q = heat flux, w/m^2
T = temperature, K
U = constant velocity in x direction, m/s
u = variable velocity in x direction, m/s
x = layer axial displacement, m
y = layer transverse displacement, m
β = extinction coefficient, m^{-1}; $=\sigma_a + \sigma_s$
ϵ_d = emissivity of a single droplet
ϵ_{eff} = effective emission coefficient of layer, $=q/\sigma T_m^4$
ϵ_w = overall emission coefficient of enclosure
θ = temperature separation variable, K
κ = transverse optical displacement, $=\beta y$
λ = axial optical displacement, $=\beta x$
λ^* = normalized optical length, $=\lambda\sigma T_i^3/\rho c_P U$
μ = direction cosine in the x-y plane
ρ = density, kg/m^3
ρ_w = diffuse reflection coefficient of enclosure
σ = Stefan-Boltzmann constant
σ_a = absorption coefficient, m^{-1}
σ_s = scattering coefficient, m^{-1}
τ_w = overall transmission coefficient of enclosure
ϕ = temperature separation variable
ω = scattering albedo

Superscripts

c = conduction
R = radiation
R^+ = radiative flux in the positive direction
R^- = radiative flux in the negative direction

Subscripts

b = blackbody
d = droplet
g = gas
i = initial
l = liquid
m = mean, mixture
o = edge of the droplet layer
w = wall

Introduction

THE liquid droplet radiator (LDR) is a configuration of heat exchanger proposed for use with spacecraft. The operating principle of an LDR is to cool the working fluid by separating it into droplets and sending these droplets on a flight through space. The droplets lose heat by radiation to the near vacuum of space and are collected for recirculation at the end of their flight. The large surface area relative to the fluid mass which results from division of the working fluid into droplets makes the LDR an attractive concept for lightweight, space-based, heat-rejection equipment. Liquid metals have been proposed as working fluids for some applications, operating at temperatures on the order of 1000 K. The general layout and operating characteristics of some proposed LDR configurations have been provided in a review paper by White.[1] Figure 1a illustrates the basic components of a rectangular-type LDR.

In the earlier proposals, the droplet flight path was to be entirely open to space. However, it has been realized that this may result in degradation of the working fluid through droplet/plasma interactions in an orbital environment. Stray droplets may also seriously contaminate the spacecraft itself.[1] A proposed solution to these difficulties is to shield the droplet flight path within an enclosure. The efficiency of such an enclosure depends on its ability to transmit and emit infrared radiation. An objective of the present analysis is to calculate the heat-rejection capability of an LDR through such an enclosure, taking into account nonuniform temperature distribu-

Received Feb. 6, 1989; revision received June 8, 1989.

*Professor, Department of Mechanical Engineering and Materials Science. Member AIAA.

†Graduate Student, Department of Mechanical Engineering and Materials Science. Student Member AIAA.

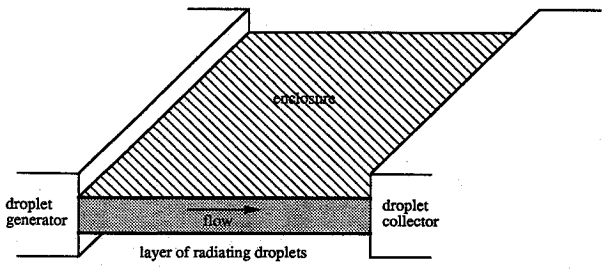

Fig. 1a Components of a liquid droplet radiator.

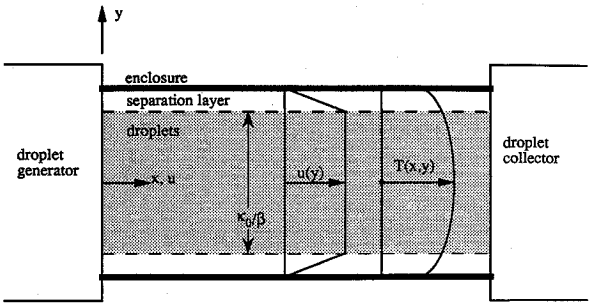

Fig. 1b Geometry of a radiating droplet sheet.

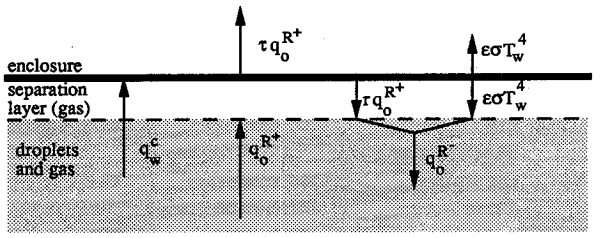

Fig. 1c Heat flux at the boundary.

tions through the thickness and along the length of the radiating droplet layer.

It is conceivable that a conductive gas may be present, interspersed among the radiating droplets. This may result from buildup of vapor within the radiating layer, or from gas injected into the layer concurrent with the droplets. For instance, an LDR with a rigid, gas-tight enclosure may be used as a heat exchanger for a power cycle in which pressure is not reduced to ambient space pressure for heat rejection. Also, gas might be purposely injected into the enclosure along with the droplets in order to control the droplet stream. The present analysis of LDR thermal performance includes the effects of thermal conductivity through a radiatively nonparticipating gas interspersed among the droplets and in local thermal equilibrium with them. This is a general problem in combined radiation/conduction heat transfer for LDR-like configurations radiating to space (no external convection). Industrial applications for the full range of parameters addressed by this analysis have yet to be proposed.

In order to maximize the total radiating surface of the droplets, a multitude of very fine droplets is preferred. In their path through space, this ensemble of droplets would appear as a clearly defined stream of a homogeneous fluid, like a mist or aerosol. Siegel[2-4] modeled this homogeneous stream as a slab or layer of a radiatively participating medium, without enclosing surfaces or gas conduction, and reached a solution using the integro-differential form of the radiative transfer equation. This technique allowed analysis of the thermal performance of an LDR using continuous radiative transfer and nonuniform temperature profiles, omitted in many earlier LDR analyses. This type of analysis confines the local effects of radiation between individual droplets to the global parameters (scattering albedo, extinction coefficient) of the homogeneous stream. In the present analysis, the first-order spherical harmonic approximation (P_1) of radiation intensity was used to express the radiation transfer relations. This allows us to express a differential set of governing equations, in which we can easily include conductive terms and enclosure boundary conditions.

In the present analysis we address the two-dimensional geometry shown in Fig. 1b, where droplets and gas are present together. It is assumed that the droplets and gas enter the layer together, in both thermal and momentum equilibrium. We have modeled the droplets as a radiatively participating, nonconducting medium, where the droplets do not contact each other. The gas is modeled as a conducting, radiatively nonparticipating medium, in local thermal equilibrium with the droplets. We suggest that a small gap may be allowed between the edge of the droplet layer and the enclosure in order to avoid wall contact by the liquid. This gap would be filled by any gas traveling with the droplets. This problem is a general one of combined radiation and convection for plane-parallel media. In the present analysis we have used radiation intensity at the enclosure wall as a boundary condition, which allows us to calculate both the wall temperatures and heat flux as parts of the solution. Previous radiation/convection analyses in plane-parallel media have specified either wall temperature or heat flux as a boundary condition.

Analysis

Governing Equation

This analysis is based on a quasi-one-dimensional treatment where the gradient of radiation and conduction heat fluxes in the downstream, or x direction, shown in Fig. 1b, are neglected in favor of gradients in the cross-stream, or y direction. Temperature is expressed as a function of both x and y. We assume local thermal equilibrium between the droplets and the gas and also assume that the liquid volume fraction is small so that conduction is carried only through the continuous gas. This results in the energy equation

$$k\frac{\partial^2 T}{\partial y^2} - \frac{\partial q^R}{\partial y} = \rho_m c_P U \frac{\partial T}{\partial x} \tag{1}$$

where ρ_m and c_P are the density and specific heat of the homogeneous layer, weighted by, respectively, the volume and mass fractions of the liquid droplets and interspersed gas. The droplets are assumed to pass along the layer with a uniform velocity U. Once this velocity has been imparted to the droplet field by the droplet generator, the droplets continue with undiminished velocity to the droplet collector.

In order to treat q^R, we employ the first-order spherical harmonic approximation (P_1) for radiation intensity. The P_1 approximation has been shown to work well in layer geometries[5] and enables us to develop a differential governing equation in place of the integro-differential expressions for general radiative transfer. The radiative transfer in plane-parallel media may be expressed as[6]

$$\frac{\partial G}{\partial \kappa} + 3q^R = 0 \tag{2a}$$

$$\frac{\partial^2 G}{\partial \kappa^2} = 3(1-\omega)(G - 4\pi I_b) \tag{2b}$$

for gray media with isotropic scattering, and where I_b is expressed as $I_b = \sigma T^4/\pi$. We have used the optical cross-stream coordinate $\kappa = \beta y$. Substituting Eqs. (2) into Eq. (1), we obtain an expression for G:

$$G = \frac{\rho_m c_p U}{(1-\omega)}\frac{\partial T}{\partial \lambda} + 4\sigma T^4 - \frac{\beta k}{(1-\omega)}\frac{\partial^2 T}{\partial \kappa^2} \tag{3}$$

where $\lambda = \beta x$. Substituting Eq. (3) into Eq. (2b) while holding ρ_m, c_P, U, ω, β, and k constant results in the governing equation

$$\frac{\partial^2}{\partial\kappa^2}\left[\frac{4}{3}\sigma T^4 + \frac{\rho_m c_P U}{3(1-\omega)}\frac{\partial T}{\partial\lambda} + \beta k T - \frac{\beta k}{3(1-\omega)}\frac{\partial^2 T}{\partial\kappa^2}\right] = \rho_m c_p U \frac{\partial T}{\partial\lambda} \tag{4}$$

Results may be expressed parametrically by re-expression of Eq. (4):

$$\frac{\partial^2}{\partial\kappa^2}\left[\frac{4}{3}\left(\frac{T}{T_i}\right)^4 + \frac{1}{3(1-\omega)}\frac{\partial}{\partial\lambda^*}\left(\frac{T}{T_i}\right) + N\left(\frac{T}{T_i}\right) - \frac{N}{3(1-\omega)}\frac{\partial^2}{\partial\kappa^2}\left(\frac{T}{T_i}\right)\right] = \frac{\partial}{\partial\lambda^*}\left(\frac{T}{T_i}\right) \tag{5}$$

where $N = \beta k/\sigma T_i^3$ is a conduction-to-radiation ratio, and $\lambda^* = \lambda\sigma T_i^3/\rho_m c_P U$ is a normalized optical length.

The volume fraction of liquid droplets in the layer is quite small, typically much less than 10^{-2}; thus its absorption and scattering characteristics may be taken from the independent scattering relations[7]:

$$\sigma_a = \frac{nD^2}{4} Q_a \tag{6a}$$

$$\sigma_s = \frac{nD^2}{4} Q_s \tag{6b}$$

For opaque spheres that are large compared to the radiation wavelength, the efficiencies may be approximated as[8]

$$Q_a = \epsilon_d \tag{7a}$$

$$Q_s = 1 - \epsilon_d \tag{7b}$$

This results in

$$\beta = \frac{nD^2}{4} \tag{8a}$$

$$\omega = 1 - \epsilon_d \tag{8b}$$

Boundary Conditions

The boundary condition requirements for solution of Eq. (4) are met by imposing centerline temperature symmetry, zero temperature slope at the centerline, radiative flux balance at the inner surface of the enclosure, and a heat balance across the enclosure wall. The enclosure wall is assumed to be thin.

The radiation heat flux at the inner surface is illustrated in Fig. 1c. Radiation heat flux travels in both directions and is expressed in P_1 as

$$q^{R+} = 2\pi\int_0^1 I\mu\, d\mu \tag{9a}$$

$$q^{R-} = 2\pi\int_0^{-1} I\mu\, d\mu \tag{9b}$$

where μ is a direction cosine in the plane of Fig. 1c, and

$$I(\kappa,\mu) = \frac{1}{4\pi}\left[G - \mu\frac{\partial G}{\partial\kappa}\right] \tag{9c}$$

Note that the limits of integration in Eq. (9b) correspond to the direction of q^{R-} shown in Fig. 1c.

The negative radiative flux at the inner surface of the enclosure is made up of reflected and emitted components; hence,

$$q_o^{R-} = \rho_w q_o^{R+} + \epsilon_w\sigma T_w^4 \tag{10a}$$

where we have assumed reflection and emission to be diffuse, and ρ_w and ϵ_w are effective reflection and emission coefficients for the entire window, as defined by Siegel and Howell.[8] The subscript o corresponds to the outer edge of the droplet stream, whereas the subscript w denotes the surface of the enclosure, a distinction that allows a temperature jump at the boundary in nonconducting cases. Substituting Eqs. (9) into Eq. (10a) results in

$$\frac{1}{4}(1-\rho_w)G_o + \frac{1}{6}(1+\rho_w)\frac{\partial G_o}{\partial\kappa} = \epsilon_w\sigma T_w^4 \tag{10b}$$

where G is given by Eq. (3). This is the intensity boundary condition for P_1 written as a Marshak boundary condition.

A heat balance across the enclosure wall may be written following Fig. 1c as

$$q_w^c + q_o^{R+} - q_o^{R-} = \tau_w q_o^{R+} + \epsilon_w\sigma T_w^4 \tag{11a}$$

where q^c represents conduction through the nonparticipating gas, expressed as $q^c = -\beta k(\partial T/\partial\kappa)$, and τ_w is the effective transmission coefficient[8] for the window. Substituting Eqs. (9) into Eq. (11a) results in

$$0 = \beta k\frac{\partial T_w}{\partial\kappa} + \epsilon_w\sigma T_w^4 + \frac{\tau_w}{4}G_o + \frac{1}{6}(2-\tau_w)\frac{\partial G_o}{\partial\kappa} \tag{11b}$$

In cases where there is no gas conductivity, the conduction terms in Eqs. (10b) and (11b) are zero, and there is a temperature jump at the boundary. The governing Eq. (4) reduces to second order for these cases. This special case may then be solved with either boundary condition, Eq. (10b) or (11b), whereas the remaining condition serves to define T_w. Solving Eqs. (10b) and (11b) using the enclosure energy balance $1 = \tau_w + \rho_w + \epsilon_w$ results in the radiative flux boundary condition

$$q^{R-} = (\rho_w + \epsilon_w/2)q^{R+} \tag{12}$$

This demonstrates that, for the nonconducting case, the effect of wall radiative properties on the radiative flux is limited to the single parameter $C = \rho_w + \epsilon_w/2$.

In cases where there is gas conductivity, there can be no temperature jump, and it is necessary to solve the temperature distribution in the small gap between the edge of the droplet stream and the inner surface of the enclosure. In this gap we can write an energy equation

$$k_g\frac{\partial^2 T}{\partial y^2} = \rho_g c_{P,g} u\frac{\partial T}{\partial x} \tag{13}$$

where $u = U(y_o - y_w)/(y_o - y_w)$. This velocity profile represents our idealizations that the droplets maintain the constant speed U imparted by the droplet generator, the gas interspersed between the droplets travels at the same speed as the droplets, and the gas flow between the droplet edge and the wall takes on a linear velocity profile. Throughout the nonparticipating gas in the gap, the radiative flux remains constant. The additional boundary conditions necessary to include Eq. (13) in the general solution are temperature and conduction heat flux matching at the interface between the droplet-gas mixture and the gas-only gap.

Numerical Solution

A fully implicit scheme, using central differences in the cross-stream direction and forward differences downstream, was used to solve the temperature profile problem of Eqs. (4) and (13), subject to matching conditions between regions and the boundary conditions of Eqs. (10) and (11). Heat flux was

then calculated using one side of Eq. (11a). A marching algorithm was employed, starting from a given initial temperature profile at the droplet generator. Each step included a linearization loop for the T^4 terms, converging to a preset accuracy (generally 0.1 K) before proceeding to the next step downstream. It was found necessary to use a variable mesh size in the cross-stream direction, with finer intervals near the enclosure walls. In order to simplify the variable mesh difference terms, auxiliary points appearing in the central differences at the boundaries were included in the problem. The boundary conditions were then written explicitly into the problem matrices.

The algorithm was programmed with a variable degree of implicitness, allowing fully explicit and semiexplicit (Crank-Nicholson) solutions. However, in practice it proved infeasible to use a downstream step size small enough to meet the stability criterion for partially explicit formulations. Therefore, all solutions were generated in the fully implicit mode.

In the fully implicit mode, approximately 15 variably spaced cross-points in the half thickness were generally sufficient to yield convergent solutions. For problems with enclosure but without conduction, approximately 10 points were necessary. Running time for the problem was generally quick enough to allow foreground operation on a superminisized processor.

Analytical Solution

For cases without conduction, Eq. (4) reduces to second order and separates when we assume a solution of the form $T(\lambda,\kappa)=\theta(\lambda)\phi(\kappa)$ and linearize ϕ^4 around $\phi(0)=1$ at the centerline, $\phi^4\approx 4\phi-3$. In this separation, θ represents the centerline temperature, and ϕ represents a nondimensional cross-stream temperature profile. The resulting separation equations are

$$\frac{\rho_m c_P U}{(1-\omega)} - 3\rho_m c_P U \frac{\phi}{d^2\phi/d\kappa^2} = M \tag{14a}$$

$$-16\sigma \frac{\theta^4}{d\theta/d\lambda} = M \tag{14b}$$

where M is the separation constant. Equation (14b) may be solved with an initial condition $\theta(0)=T_i$, resulting in

$$\theta(\lambda) = \left(48\frac{\sigma}{M}\lambda + T_i^{-3}\right)^{-1/3} \tag{15a}$$

Equation (14a) has a solution of the general form $\phi=c_1\sin(m\kappa)+c_2\cos(m\kappa)$. Using boundary conditions $\phi(0)=1$ and $d\phi/d\kappa(0)=0$, we have

$$\phi = \cos(m\kappa) \tag{15b}$$

where

$$m = \left[\frac{M}{3\rho_m c_P U} - \frac{1}{3(1-\omega)}\right]^{-1/2} \tag{15c}$$

In order to express results in terms of the mean temperature of the profile, we employ

$$\phi_m = \frac{2}{\kappa_o}\int_0^{\kappa_o/2}\cos(m\kappa)\,d\kappa = \frac{2}{m\kappa_o}\sin(m\kappa_o/2) \tag{16}$$

where the mean temperature is expressed as $T_m=\theta\phi_m$.

The boundary conditions (10) and (11) may be combined to eliminate T_w with the result (using $1=\tau_w+\rho_w+\epsilon_w$)

$$(1-\rho_w-\epsilon_w/2)G_o + \frac{2}{3}(1+\rho_w+\epsilon_w/2)\frac{\partial G_o}{\partial\kappa} = 0 \tag{17a}$$

where the terms in parentheses may be recognized as $(1-C)$ and $(1+C)$. After some rearrangement using Eqs. (3) and (15), we have an implicit equation for m:

$$\cos(m\kappa_o/2) = \frac{2(1+\rho_w+\epsilon_w/2)}{3(1-\rho_w-\epsilon_w/2)} m\sin(m\kappa_o/2) + \frac{3}{4}\left[1+\frac{m^2}{3(1-\omega)}\right] \tag{17b}$$

This solution represents an extension of the technique presented by Bayazitoglu and Jones[9] to LDR cases with an enclosure. The heat flux from either side of the LDR may be reduced from this analysis using Eqs. (3), (9), and (11), resulting in

$$\frac{q}{\sigma\theta^4} = \frac{16m\sin(m\kappa_o/2)}{3+m^2/(1-\omega)} \tag{18}$$

Heat flux results for LDR's are often expressed as an effective emissivity for the layer, $\epsilon_{\text{eff}}=q/\sigma T_m^4$. For this result, Eq. (18) must be divided by the linearization $\phi_m^4\approx 4\phi_m-3$ to produce ϵ_{eff}.

Results and Discussion

In order to validate our results, temperature profiles were compared with the results of previous studies. The profiles presented by Siegel[2-4] and Mattick and Hertzberg[10] correspond to the special case of a nonconducting gas with no enclosure. Temperature profiles generated by the numerical solution compared well with the previous studies, with the exception of slightly higher temperatures at the layer boundaries in optically thin cases with low-scattering albedos. This is thought to be a difficulty with boundary condition representation for the P_1 approximation and may lead to almost 10% higher heat flux results than for exact solutions in thin, low-scattering cases. Temperature profiles generated by the analytical solution roughly overlap the numerical profiles, but with a slightly different shape. This is due to the linearization of the ϕ^4 terms and the resulting trigonometric form enforced by Eq. (15b). However, heat flux results from both the analytical and numerical profiles compare very closely. The downstream temperature decay also compared favorably with the results of Siegel[2] for both the analytical and numerical methods.

The separated analytical solution assumes that the temperature maintains a similar profile as the droplets move downstream. Siegel[2-4] studied LDR's without enclosures and found that similar profiles would be reached after a suitable development length. For these similar profiles, the locally nondimensionalized heat flux is constant with downstream distance. It has been found in the present and previous anslyses[2,10] that the heat flux in the developing region is greater than in the fully developed region by small amounts, on the order of 2-10%. The lower figure applies to optically thin layers. Fully developed results from both the analytical and numerical solution methods are presented here, with the understanding that these results are slightly conservative.

Enclosed LDR without Conduction

The effect of an enclosure on nonconducting LDR's is confined to variations in the parameter $C=\rho_w+\epsilon_w/2$, as demonstrated by Eq. (12). The C varies in the range from 0 to 1, where $C=0$ corresponds to a fully transmissive enclosure ($\tau_w=1$), $C=0.5$ is a fully emissive (black) enclosure ($\epsilon_w=1$), and $C=1$ is a fully reflective enclosure ($\rho_w=1$), for which $\epsilon_{\text{eff}}=0$. Figure 2a shows the effect of C on the relation of ϵ_{eff} to optical thickness for a scattering albedo of 0.5. At peak values, the reduction in ϵ_{eff} is nearly in proportion to C. However, at optical thicknesses above and below κ_o for peak ϵ_{eff}, the reduction is less, with the result that ϵ_{eff} for an enclosed LDR is more constant with optical thickness than that for a nonenclosed LDR. Many of the liquids proposed for LDR's have droplet emissivities on the order of 0.1,[10] corresponding

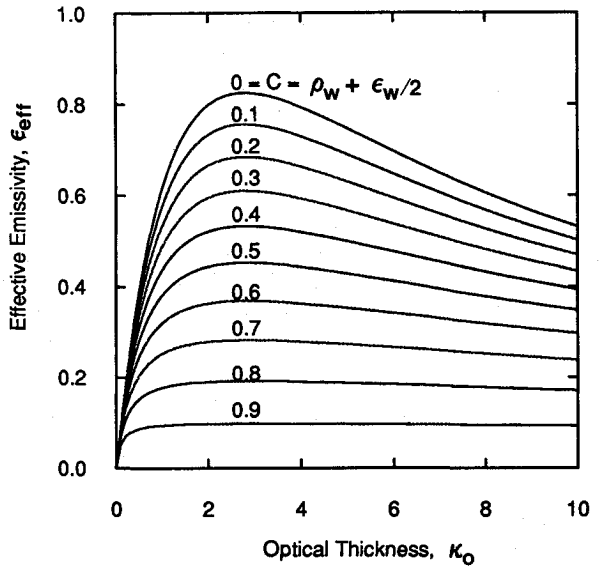

Fig. 2a Effective emissivity of an enclosed radiating droplet sheet for $\omega = 0.5$.

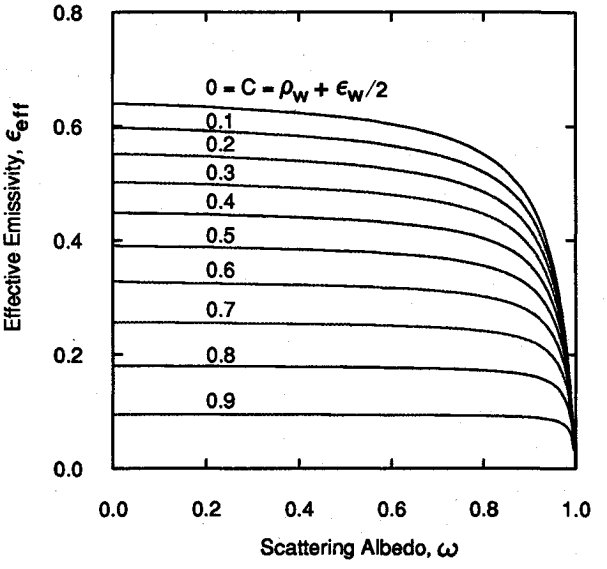

Fig. 3a Effective emissivity of an enclosed radiating droplet sheet for $\omega = 1 - \frac{1}{2}\kappa_o$.

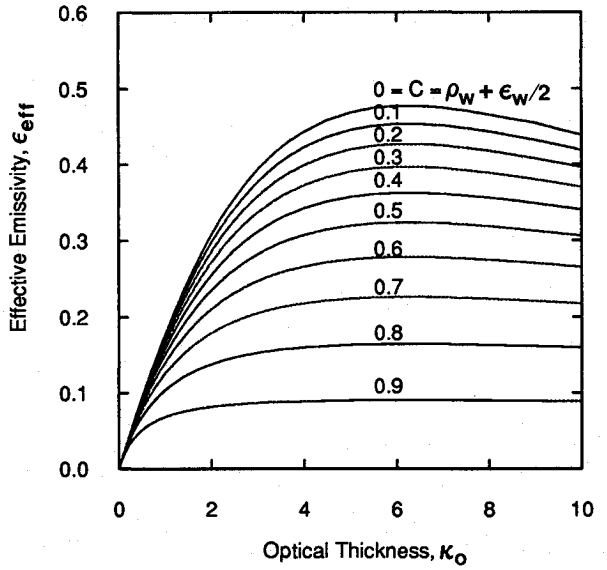

Fig. 2b Effective emissivity of an enclosed radiating droplet sheet for $\omega = 0.9$.

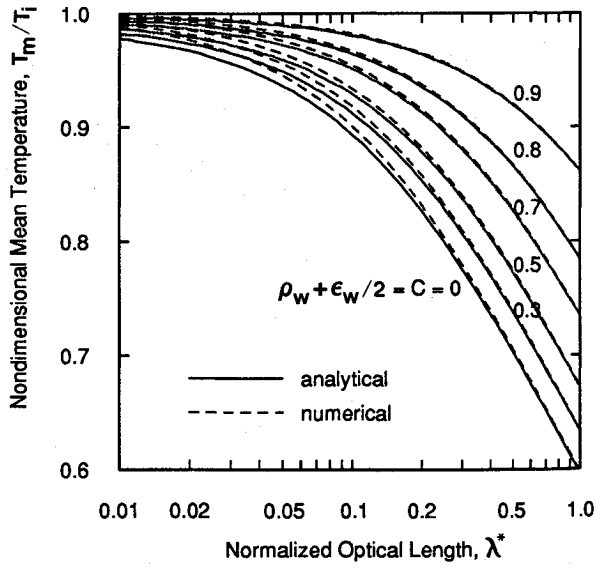

Fig. 3b Mean temperature of an enclosed radiating droplet sheet for $\omega = 0.5$ and $\kappa_o = 1$.

through Eq. (7b) to an albedo of 0.9. Figure 2b shows the effect of C on ϵ_{eff} for $\omega = 0.9$. The effect of enclosure properties is less pronounced at a higher ω, with ϵ_{eff} for the emissive (black) enclosure case approximately 70% of that for the fully transmissive case.

In specifying the dimensions of an LDR, the mass of piping and droplet generating and collecting equipment must be considered in order to preserve the LDR's weight advantage over other space-based heat-rejection configurations. Therefore, for a given scattering albedo, the optical thickness cannot be varied independently to yield the highest effective emissivity. Mattick and Hertzberg[10] have suggested that, on the basis of minimizing the ratio of device mass to heat-rejection rate, the best results can be achieved by an LDR where $\kappa_o = \frac{1}{2}\epsilon_d$. Figure 3a shows ϵ_{eff} resulting from the relation $\kappa_o = \frac{1}{2}(1-\omega)$ for the range of C, given as a function of ω. For low- and midrange values of ω (higher ϵ_d), ϵ_{eff} is relatively constant. At high values of ω (lower ϵ_d), ϵ_{eff} falls off rapidly to the limit $\epsilon_{eff} = 0$ at $\epsilon_d = 0$.

For all of the cases shown in Figs. (2) and (3), ϵ_{eff} at the initial condition is only very slightly higher than ϵ_{eff} for the fully developed profile. Figures 2 and 3 show only results from the analytical method for clarity. Results from the numerical method correspond very closely to the analytical method results.

Decreasing the effective emissivity by increasing the thermal resistance of the enclosure has the complementary effect of decreasing the loss of mean temperature in the layer. Figure 3b shows the mean temperature (nondimensionalized by the initial temperature) as a function of λ^* for the range of C and an albedo $\omega = 0.5$. Figure 3b shows results from both the analytical and numerical methods. Agreement between the two methods is fairly good. The numerical method is sensitive to the step size, $\Delta\lambda^*$, and particularly so near the initial point. The results shown in Fig. 3b were computed with $\Delta\lambda^* = 0.001$. Correlation between the analytical and numerical method results may be improved by reduction of this step size.

Enclosed LDR with Conduction

The general effect of conduction in the radiating droplet layer is to spread the temperature more evenly across the profile, as a result of the additional mechanism for heat transfer. This increases the heat flux from the layer relative to a given

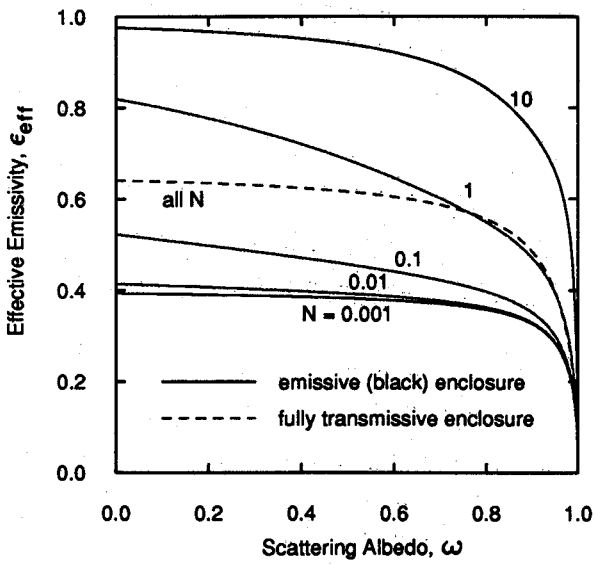

Fig. 4a Effective emissivity of an enclosed radiating droplet sheet with conduction for $\lambda^* = 0.1$ and $\omega = 1 - \frac{1}{2}\kappa_o$.

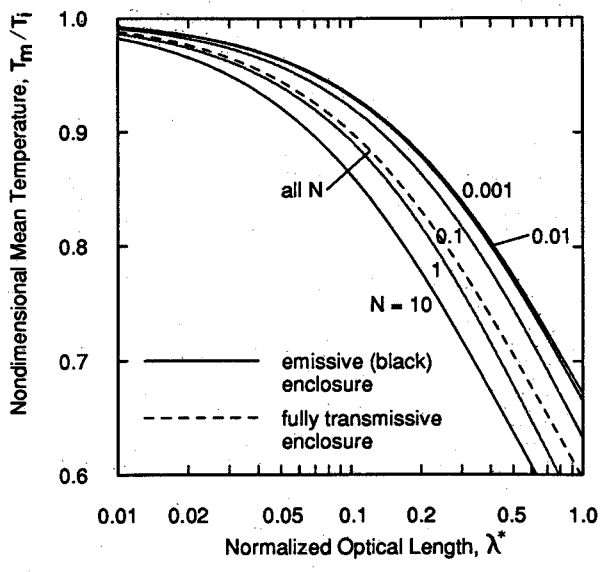

Fig. 4b Mean temperature of an enclosed radiating droplet sheet with conduction for $\omega = 0.5$ and $\kappa_o = 1$.

centerline temperature by increasing the temperature at the boundaries. Introduction of a conductive gas into a given array of droplets has the further effects of increasing the mixture density ρ_m. Increasing the mixture density has the effect of shifting a no-gas effective emissivity curve to the right when plotted against a dimensional length.

When expressed as a function of N and λ^*, the addition of a conductive gas has very little effect on the effective emissivity for $N < 0.01$ and almost no effect for $N < 0.001$. Therefore, for nonpressurized LDR configurations, conduction effects are not important, since the space ambient pressure gives rise to very low values of N. However, a purpose of this analysis is to address radiation and conduction in a gas droplet layer radiating to space as a general problem, for future application to internally pressurized or other LDR-like configurations that may have high values of N.

For higher values of N, the effect of conduction is found to result from the radiative properties of the enclosure. The presence of the conductive term in the boundary condition (11) prevents the simplification of Eq. (12); hence, the enclosure may not be summarized in terms of the parameter C. However, the influence of enclosure properties may be simply illustrated by the special cases of a fully transmissive ($\tau_w = 1$, $\epsilon_w = 0$, $\rho_w = 0$) and of an emissive (black: $\tau_w = 0$, $\epsilon_w = 1$, $\rho_w = 0$) enclosure. For the fully transmissive enclosure, the boundary conditions (10) and (11) reduce to

$$\frac{1}{2} G_o + \frac{1}{6} \frac{\partial G_o}{\partial \kappa} = 0 \tag{19a}$$

$$N \frac{\partial T_w}{\partial \kappa} = 0 \tag{19b}$$

which represent the nonenclosed Marshak condition with conductive equilibrium. In practice, the effect of Eq. (19b) for $N \neq 0$ is contained within the separation layer of gas between the gas droplet mixture and the enclosure wall. Increasing N spreads the temperature profile more evenly within the droplet layer, although the effect on overall effective emissivity is negligible. For the emissive (black) enclosure, the boundary conditions (10) and (11) reduce to

$$\frac{1}{4} G_o + \frac{1}{6} \frac{\partial G_o}{\partial \kappa} = \epsilon_w \sigma T_w^4 \tag{20a}$$

$$\beta k \frac{\partial T_w}{\partial \kappa} + \frac{1}{4} G_o + \frac{1}{2} \frac{\partial G_o}{\partial \kappa} = 0 \tag{20b}$$

Equations (20) have a significant effect on ϵ_{eff} for $N > 0.01$. The general effect of conductivity for this case, compared to nonconducting results, is for ϵ_{eff} to take on a higher initial value, decline slightly along with the developing profile, and then gradually increase to an asymptotic value for very large λ^*. Within the range of λ^* of practical interest (dimensional heat flux still a significant fraction of its initial value), ϵ_{eff} may be regarded as roughly constant with respect to λ^*.

Figure 4a shows the effective emissivity for both fully transmissive and emissive (black) enclosures for a range of N at $\lambda^* = 0.1$, using the relation $\kappa_o = \frac{1}{2}(1 - \omega)$. These curves were generated for a gap between the droplet layer and the wall of 10% of the droplet layer thickness, $\rho_l = 1000\rho_g$, and $c_{P,l} = c_{P,g}$. For the fully transmissive case, Fig. 4a shows no effect for changes in N. The fully transmissive curve corresponds to the $C = 0$ curve in Fig. 3a. For the emissive (black) case, the effect of conduction is negligible for $N < 0.001$. The $N = 0.001$ curve corresponds to the $C = 0.5$ curve in Fig. 3a. As N increases from 0.01, the effective emissivity increases dramatically until it is near 1.0 for most values of the scattering albedo at $N = 10$. If Fig. 4a were to be redrawn at increasing values of λ^*, the ϵ_{eff} curves would rise from the $N = 0.001$ curve toward the $N = 10$ curve (which approximate the limits of variation of ϵ_{eff} with N). However, this rise is slow within the range of λ^* of interest. At $\lambda^* = 1.0$ the $N = 1$ curve is about 25% higher than at $\lambda^* = 0.1$, the $N = 0.1$ curve is about 10% higher, and the other curves are nearly unchanged.

Figure 4b shows the complementary decrease in mean temperature as a function of normalized optical length with increasing N for fully transmissive and emissive (black) enclosures and $\omega = 0.5$. The fully transmissive curve corresponds to the $C = 0$ curve in Fig. 3b. The $N = 0.001$ curve for the emissive (black) enclosure corresponds to the $C = 0.5$ curve in Fig. 3b, but for this N there is negligible effect of conduction. As N is increased from 0.01 there is a decline in mean temperature as a result of the increasing effective emissivities shown in Fig. 4a.

Conclusions

From the results of the numerical and analytical solutions presented here, we can conclude the following:

1) An analytical solution for rectangular-type LDR's enclosed within transmitting, emitting, and reflecting boundaries has been given. This solution compares well with numerical solutions for fully developed temperature profiles. The analytical solution presented here is recommended for use in rectangular-type LDR performance evaluation, without con-

sideration of developing profile effects. Such analyses will be slightly conservative.

2) Enclosing an LDR within transmissive/emissive boundaries decreases its heat-rejection capability as a function of the parameter $C = \rho_w + \epsilon_w/2$, where ρ_w and ϵ_w are the overall reflection and emission coefficients of the enclosure. For an emissive (black) enclosure, the heat rejection is between 50 and 70% that from a fully transmissive enclosure or a nonenclosed LDR.

3) A flow of conductive, radiatively nonparticipating gas interspersed among the droplets in an LDR will have negligible effect on its heat-rejection capability, apart from its effect in increasing the thermal storage of the layer, if N is less than 0.01. For $N > 0.01$, the overall effect of conduction depends on the enclosure materials. For fully transmissive enclosures, the effect continues to be negligible for optical lengths of practical interest. For emissive (black) enclosures, high values of N have a strong positive effect on heat rejection. Partially transmisive enclosures may be expected to scale between these extremes.

References

[1]White, K. A. III, "Liquid Droplet Radiator Development Status," AIAA Paper 87-1537, July 1987; also NASA TM-89852.

[2]Siegel, R., "Transient Radiative Cooling of a Droplet-Filled Layer," *Journal of Heat Transfer,* Vol. 109, No. 1, 1987, pp. 159–164.

[3]Siegel, R., "Radiative Cooling of a Layer with Nonuniform Velocity—a Separable Solution," *Journal of Thermophysics and Heat Transfer,* Vol. 1, No. 3, 1987, pp. 228–232.

[4]Siegel, R., "A Separation of Variables Solution for Nonlinear Radiative Cooling," *International Journal of Heat and Mass Transfer,* Vol. 30, No. 5, 1987, pp. 959–966.

[5]Bayazitoglu, Y. and Higenyi, J. K. D., "Higher-Order Differential Equations of Radiative Transfer: P_3 Approximation," *AIAA Journal,* Vol. 17, 1979, pp. 424–431.

[6]Ozisik, M. N., *Radiative Transfer,* Wiley, New York, 1973, pp. 334–343.

[7]Tien, C. L., "Thermal Radiation in Packed and Fluidized Beds," *Journal of Heat Transfer,* Vol. 110, 1988, pp. 1230–1242.

[8]Siegel, R. and Howell, J. R., *Thermal Radiation Heat Transfer,* 2nd ed., Hemisphere, Washington, DC, 1981, pp. 152–158 and 721–731.

[9]Bayazitoglu, Y. and Jones, P. D., "Radiative Cooling of a Liquid Droplet-Gas Layer," *ASME Proceedings of the 1988 National Heat Transfer Conference,* v. 1, pp. 193–199, HTD-Vol. 96, ASME, New York, 1988.

[10]Mattick, A. T. and Hertzberg, A., "Liquid Droplet Radiator Performance Studies" *Acta Astronautica,* Vol. 12, No. 7/8, 1985, pp. 591–598.